The Hydrodynamics of Flow Stimuli

Matthew J. McHenry and James C. Liao

Keywords Boundary layer • Hair cell • Kármán gait • Lateral line • Localization • Neuromast • Predation • Reynolds number • Rheotaxis • Swimming • Turbulence • Vortex street • Unsteady flow

1 Introduction

The lateral line system allows a fish to respond to changes in its surroundings by detecting flow stimuli. The velocity, acceleration, pressure gradient, and shear stress of water at the surface of a fish may all serve as stimuli that yield cues about environmental change. All of these stimuli are governed by hydrodynamics. Therefore, an application of hydrodynamic principles offers insight into the information provided by the lateral line system. The present chapter aims to explain these principles and to illustrate how they may be applied to understand the role of the lateral line system in fish behavior.

M.J. McHenry (✉)
Department of Ecology & Evolutionary Biology, University of California, 321 Steinhaus Hall, Irvine, CA 92697, USA
e-mail: mmchenry@uci.edu

J.C. Liao
The Whitney Laboratory for Marine Bioscience, Department of Biology, University of Florida, 9505 Ocean Shore Blvd., St., Augustine, FL 32080, USA

2 Hydrodynamic Principles

Hydrodynamic theory is concerned with the forces generated by water motion. Although this motion can be highly complex, it emerges from just two fundamental fluid forces. Inertial force is generated by the acceleration of water. Viscous force is created by a fluid's ability to adhere to itself and to surfaces. The relative magnitude of these forces, as estimated by the Reynolds number, indicates where a flow resides in a continuum between perfectly smooth (i.e., viscous-dominated) and completely turbulent (i.e., inertia-dominated). For the present discussion, the Reynolds number provides a major indicator of the nature of flow at the surface of the body, where flow stimuli are detected by mechanosensory neuromasts.

2.1 *Dynamic Properties of a Fluid*

Any flow field may be thought of as a tremendous number of infinitesimal volumes, each of which approximates a cube. These fluid cubes exert forces on one another and the obstacles that they encounter. Imagine extracting one of these cubes and suspending it in space under zero gravity. If you were to push the cube with your finger, it would accelerate at a rate determined by the force that you exert upon it, as predicted by Newton's Second Law:

$$\text{Force} = \text{mass} \times \text{acceleration}. \tag{1}$$

This equation can be reformulated to apply more broadly to fluid flows. The mass of the cube is equal to the product of its density (ρ) and infinitesimal volume (dV) (Fig. 1a). This volume is equal to the product of the area upon which the force acts (dS) and the linear dimension (dx) in the direction of the force (i.e., along the x- axis, Fig. 1a). When surrounded by water in a flow field, the cube's acceleration (du/dt) is created by a difference in the pressures acting to propel and resist the cube's motion (dp). Therefore, Eq. (1) for a volume of fluid may be rewritten as follows (Batchelor, 1967):

$$dp/dx = -\rho du/dt. \tag{2}$$

This relationship, one form of the Euler equations, has implications for flow sensing. For example, it indicates that fluid acceleration varies with the pressure gradient. This explains why canal neuromasts, which are sensitive to pressure gradients, are often described as acceleration detectors (see Section 3 and the chapter by van Netten & McHenry). However, a major assumption of this flow model is that the viscosity of the water may be neglected. Inviscid models are
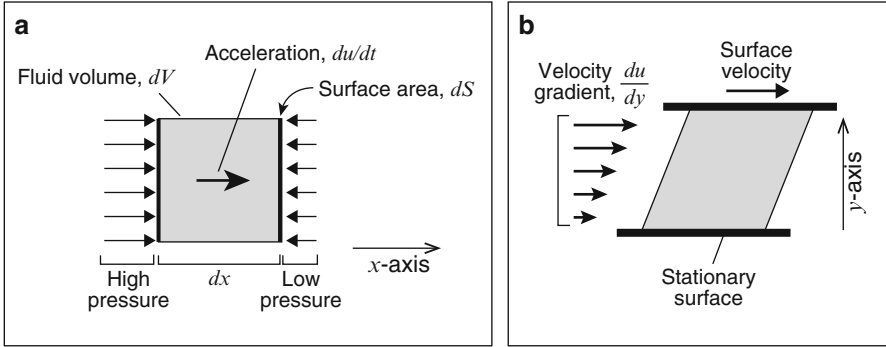
Fig. 1 The dynamic properties of a fluid. (**a**) A volume of fluid (gray box) accelerates in a pressure gradient (dp/dx, Eq. 2), which here decreases along the x-axis. (**b**) Shearing is generated in the fluid between two parallel surfaces (Eq. 3). In the case pictured, the top surface moves at a velocity parallel to a stationary surface. Fluid adhering to both surfaces creates a velocity gradient (du/dy)

reasonable under some conditions that are relevant to the lateral line system (see Section 4.1), but viscosity plays a key role in many aspects of flow sensing (see Sections 4.2 and 4.3).

Viscosity causes a fluid to resist shearing, which can be understood by returning to our virtual experiment. Imagine sliding a small volume of water between your forefinger and thumb. This motion causes the surface of your fingers to shear the fluid as they apply force directed parallel to the direction of motion (Fig. 1b). This force is proportional to both the rate of sliding between your fingers and water's viscosity. It is therefore not surprising that honey, with a relatively high viscosity, would be easier to feel between your fingers than water. Viscosity causes a fluid to adhere to a surface and thereby causes your forefinger to carry a layer of fluid as it slides in one direction and another layer to adhere to your thumb, moving in the opposite direction. This generates a gradient in flow velocity (du/dy), where y is perpendicular to the surfaces) in the space between your fingers (Fig. 1b). The force that creates this gradient per unit area of fluid is known as the shear stress (τ, with units of Pa) and it is proportional to the dynamic viscosity of the fluid (μ):

$$\tau = \mu \ du/dy. \tag{3}$$

This relationship, known as Newton's law of friction (Schlichting, 1979), demonstrates how shear stress relates to a spatial gradient in velocity. It follows that a steep gradient in flow velocity makes a relatively large contribution to the viscous force that may act on a submerged body.
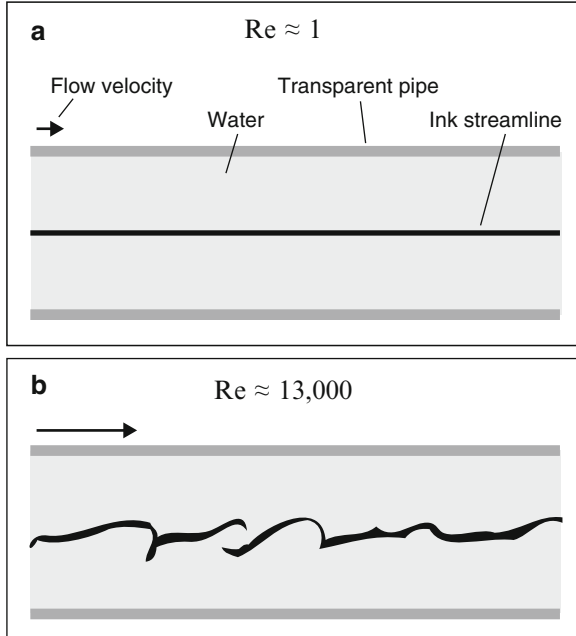
a Re ≈ 1

Flow velocity Transparent pipe

Water Ink streamline

b Re ≈ 13,000

Fig. 2 Flow patterns vary with Reynolds number (Re). This principle was illustrated by the experiments of Osborne Reynolds, who examined flow through the center of a glass cylinder by means of an ink streamline, which is shown schematically here. (**a**) At relatively low Re values, the ink passes through the pipe as a straight line due to the laminar flow throughout its cross-section. (**b**) If flow speed is increased, higher Reynolds numbers are attained (Eq. 4) and the flow becomes turbulent at Re > 13,000 but may occur lower values due the geometry and texture of the surface over which the water flows (Reynolds, 1883; Van Dyke, 1982)

2.2 Reynolds Number

Flow patterns vary with the relative magnitude of viscous and inertial forces. As demonstrated by Osborne Reynolds, turbulence occurs when inertial forces are substantially greater than viscous forces (Reynolds, 1883). Reynolds found that flow is distinctly non-turbulent at low speeds or in liquids with a high viscosity (Fig. 2a) (Van Dyke, 1982). In this condition, known as laminar flow, the water throughout a pipe's cross section is directed downstream without lateral motion. Reynolds found that laminar flow could become turbulent by increasing flow speed, pipe diameter, or the density of water (Fig. 2b). He deduced that turbulence consistently appeared at a particular value of the following ratio of these parameters:

$$Re = \rho u l / \mu, \tag{4}$$

where l is a characteristic length (e.g., the diameter of a pipe). This ratio, now known as the Reynolds number, may be mathematically derived (from Eqs. 2 and 3) as the ratio of inertial to viscous force (Schlichting, 1979). Therefore, Re indicates the hydrodynamic regime of a flow field by approximating the relative magnitude of these forces.

The Reynolds number serves as a key hydrodynamic index that may be easily calculated from measurements of length and speed. For example, the Reynolds number for a gliding fish (e.g., *Astyanax fasciatus;* Windsor et al., 2008) can be computed using the body length, gliding speed ($l = 5$ cm, $u = 12$ cm s^{-1}), and known physical properties of water ($\rho \approx 1000$ kg m^{-3}, $\mu \approx 0.001$ Pa s). The resulting value (Re ≈ 6000) suggests that the inertial force is dominant in determining the flow around the body. In this regime, models that neglect viscosity may predict large-scale flow patterns with reasonable accuracy.

Reynolds number calculations demonstrate how flow sensing is affected by hydrodynamics at multiple levels of organization. In the example of the gliding fish considered above, the Re value for a superficial neuromast on the rostrum uses the diameter of the neuromast as the characteristic length ($l \approx 10$ μm). Using the same speed of gliding and physical constants as above yields a low Reynolds number value (Re ≈ 1.2), which indicates that viscous forces are of a significant magnitude to flow at the receptor level.

2.3 *Viscous Boundary Layers*

Flow is sensed at the surface of a fish's body and viscosity plays a key role at this interface. By adhering to the surface, a spatial gradient in velocity is created between the surface and freestream flow. This gradient, known as the boundary layer, varies with the nature of freestream flow and the shape of the body. For a flat surface, boundary layers created by unidirectional or oscillating flows are well characterized by classical mathematical models (Prandtl, 1904; Schlichting, 1979). These models offer a first-order approximation of water motion over a fish's body that may be detected by the lateral line system.

The creation of a boundary layer is most easily understood for unidirectional flow, as seen in gliding fish (Daniel, 1981; Anderson et al., 2001). As a fish glides forward, water moves over the body in the opposite direction, like stacked layers running parallel to the surface. Before encountering the fish, these layers travel together with equal velocity and consequently displace over an equivalent distance for an interval of time (Fig. 3a*i*). As this fluid encounters the body, viscous adhesion slows the layer closest to the surface and thereby reduces its displacement (Fig. 3a*ii*). As the fluid continues to move along, layers further away are eventually slowed by the fluid closest to the surface (Fig. 3a*iii–iv*). This process establishes a spatial gradient of monotonically increasing velocity with distance from the surface (Fig. 3b). The distance from the surface where velocity is nearly equal to the freestream (u_∞) is called the boundary layer thickness (δ_{DC}). This is commonly
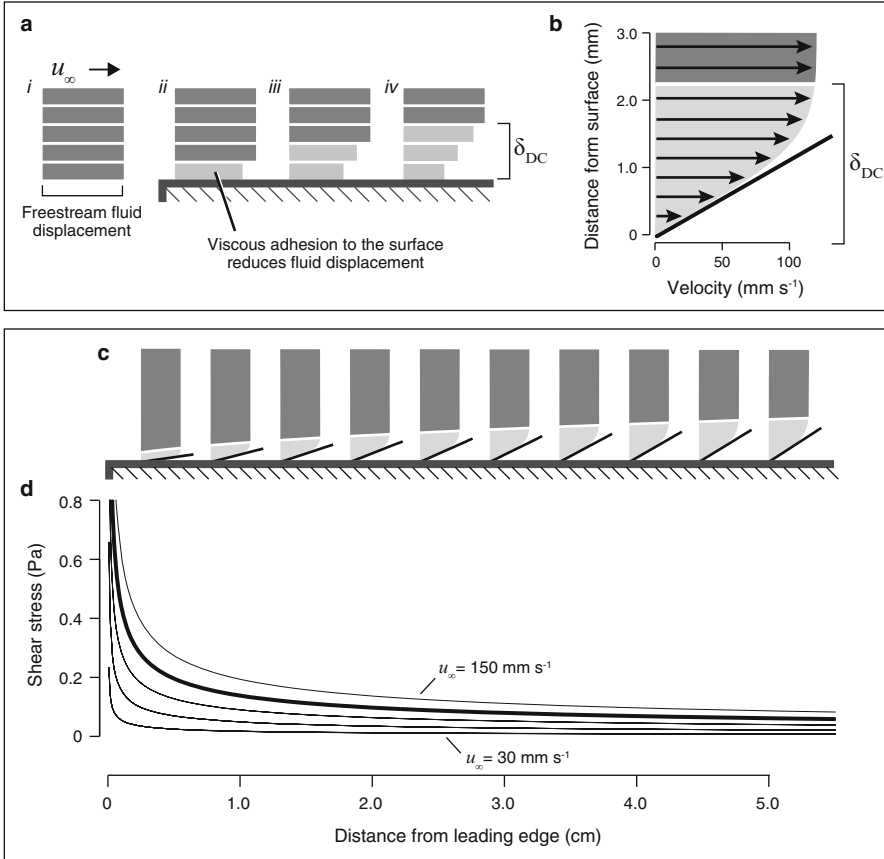
Fig. 3 The viscous boundary layer over a flat plate in unidirectional flow. (**a**) A schematic illustration of the displacement of layers of fluid as they move right-ward, over a flat surface. (*i*) Before encountering the surface, all layers of fluid displace by an equal amount for some interval of time (denoted by the horizontal length of each dark gray bar), determined by the freestream velocity, u_∞. (*ii*) As this fluid moves over the surface, the layer closest to the surface adheres to it and displaces less (light gray bar) than layers further away. (*iii*) Viscous adhesion between layers reduces the displacement of the layers further from the surface. (*iv*) This process proceeds to create the boundary layer, which is reflected in a gradient of displacement that increases with distance from the surface. (**b**) A boundary layer consequently exhibits a monotonic increase in velocity with distance. The boundary layer thickness (δ_{DC}) occurs at a distance at which the velocity is close to the freestream value. The shear stress at the surface is inversely proportional to the slope of the tangent line drawn for the velocity gradient. (**c**) A series of these tangent lines illustrates how the shear stress reduces as water moves further along a surface. This occurs while the boundary layer thickness (light gray region) increases. (**d**) The change in shear stress is shown as a function of position along the plate for variable freestream velocity (in increments of 30 mm s^{-1}) for the surface in (**c**)

defined as either $\delta_{DC} = 0.99u_{\infty}$ (used presently) or $\delta_{DC} = 0.90u_{\infty}$ (Batchelor, 1967). The boundary layer thickness increases with position along the surface (Fig. 3a, c), as indicated by the following relationship, derived from a consideration of viscous forces (Schlichting, 1979):

$$\delta_{DC} = 5\sqrt{\frac{\mu x}{\rho u_{\infty}}}, \tag{5}$$

where x is the distance along the surface from the leading edge.

Superficial neuromasts protruding from the surface of the body generally must detect a stimulus from within the boundary layer, where they are deflected by viscous drag (McHenry et al., 2008). This force varies with the velocity of flow, which depends on the height from the surface due to the boundary layer (see the chapter by van Netten & McHenry). The shear stress at the surface also varies with viscosity and the velocity gradient at the surface (Eq. 3) and thereby approximates the stimulus detected by a superficial neuromast (Rapo et al., 2009; Windsor & McHenry, 2009). For unidirectional flow over a flat plate (Fig. 3d), the shear stress is given by the following equation (Schlichting, 1979):

$$\tau_{surf} = 0.332\sqrt{\frac{\mu \rho u_{\infty}}{x}}. \tag{6}$$

Assuming the body's surface is nearly flat, this relationship indicates how the shear stress decreases with the velocity gradient along the body (Fig. 3c).

The boundary layer generated by oscillatory flow has a displacement amplitude that decreases at close proximity to the surface (Fig. 4a, b). The viscous interaction with the surface also creates a phase shift in the timing of velocity of up to 45° with respect to freestream flow (Fig. 4c). As a consequence, there are moments in an oscillation when the fluid close to the surface flows in the opposite direction from the freestream (e.g., at 1.7 ms and 6.7 ms in Fig. 4a). This variation in amplitude and phase emerges from the following model of the boundary layer profile for a pressure field over a flat plate (Batchelor, 1967; van Netten, 2006):

$$u(y, \omega, t) = u_{\infty} \cos(\omega t) - u_{\infty} \exp\left(-\frac{y}{\delta_{AC}}\right) \cos\left(\omega t - \frac{y}{\delta_{AC}}\right), \tag{7}$$

where δ_{AC} is the boundary layer thickness for oscillatory flow. This boundary layer thickness is defined as follows:

$$\delta_{AC} = \sqrt{\frac{2\mu}{\rho\omega}}. \tag{8}$$

The amplitude and phase of velocity within the boundary layer varies with the frequency of oscillation (Fig. 4a–c). At relatively high frequencies, inertial forces
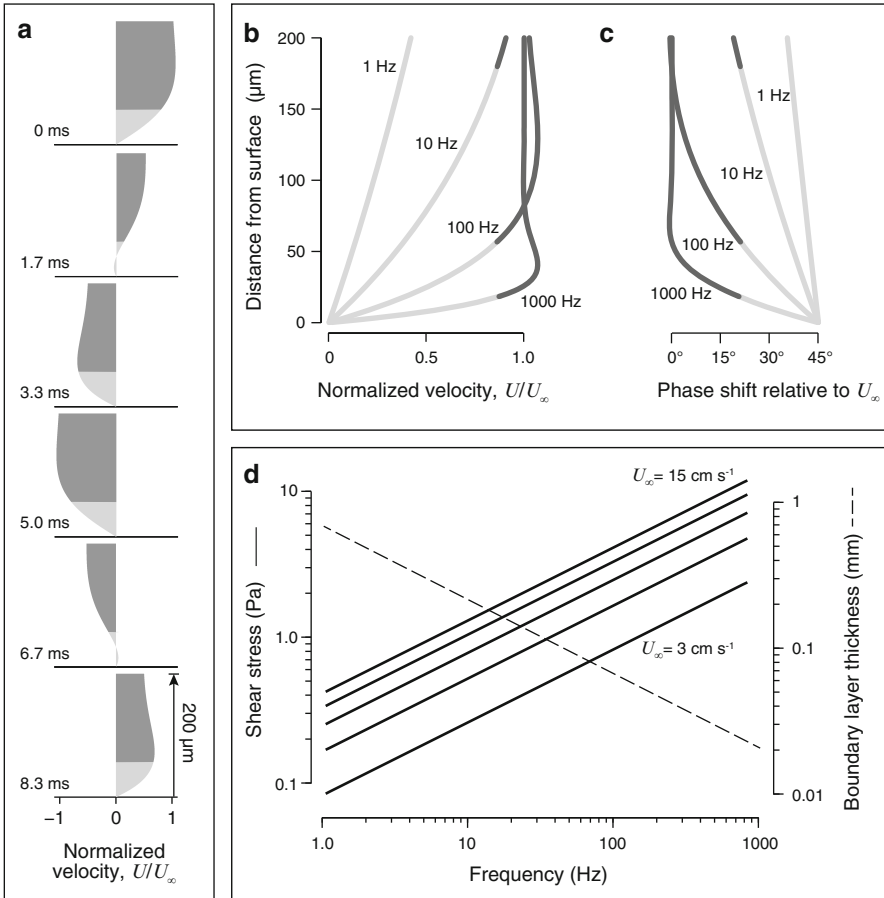
Fig. 4 The boundary layer over a flat plate in oscillating flow. (**a**) The boundary layer creates variation in the amplitude and timing of flow velocity as a function for distance from the surface. (**a–c**) The boundary layer thickness (δ_{AC}, Eq. 8) is denoted in light gray. Variation in (**b**) amplitude and (**c**) phase are shown as a function of distance from the surface for a variety of stimulus frequencies. (**d**) The surface shear stress (solid lines) and boundary layer thickness (dashed line) vary with stimulus frequency. The shear stress also varies with the amplitude of freestream velocity, as illustrated by the curves generated by stimuli ranging between 3 cm s^{-1} and 15 cm s^{-1} in 3 cm s^{-1} intervals

become more important and thereby reduce the boundary layer thickness (Eq. 8). As a consequence, the shear stress at the surface increases 10-fold over an increase in stimulus frequency from 1 Hz to 100 Hz (Fig. 4d), which is a range that encompasses the sensitivity of superficial neuromasts (McHenry et al., 2008). Therefore, the boundary layer serves as a mechanical filter that attenuates flow velocity for superficial neuromasts to an increasing degree at lower frequencies (see the chapter by van Netten & McHenry for details).
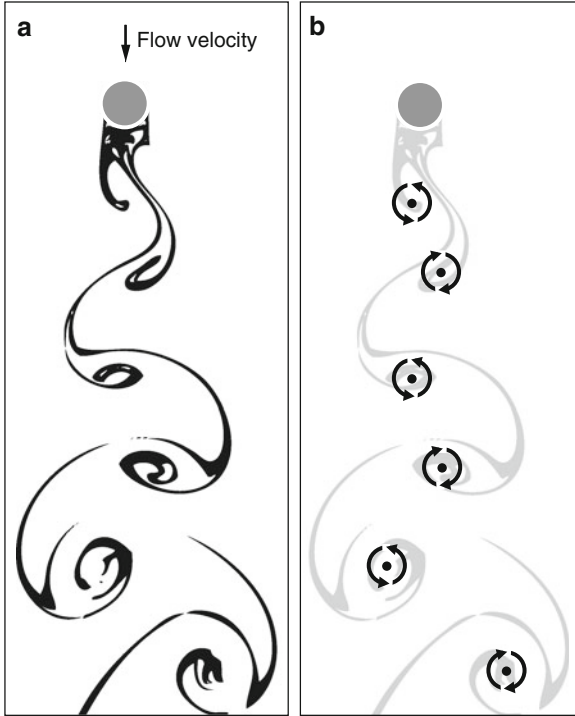
Fig. 5 The Kármán vortex street in the wake of a cylinder. (**a**) The wake behind a cylinder (gray circle) was visualized with smoke (in black) that was illuminated with a light sheet at Re = 140 (Van Dyke, 1982). (**b**) The vortex street is redrawn (in light gray) to illustrate the centers of vorticity within the drag wake (filled circles). The handedness of this vorticity (denoted by black arrows) alternates as vortices are shed on the left and right sides of the cylinder. Once shed, vortices are transported downstream with regular spacing in the direction of flow velocity

2.4 Vortices and Turbulence

Flow in a fish's environment is generally not unidirectional, nor does it oscillate at a single frequency, but is rather a heterogeneous combination of stimuli. This turbulence may provide a fish with information about environmental conditions or may hinder flow sensing by providing a source of noise. The chaos inherent to turbulence makes it a challenging frontier of fluid dynamics research (Muddada & Patnaik, 2011) and becomes an even more complicated subject when the flow field interacts with an animal's body. However, it is possible to create coherent vortices that provide a tractable means to study their influence on flow sensing and behavior (Sutterlin & Waddy, 1975; Webb, 1998; Liao et al., 2003a; Montgomery et al., 2003).

A stationary bluff body (e.g., a cylinder) in rapid flow creates a turbulent wake with a periodic shedding of vortices (Fig. 5). This trail of vorticity, called a Kármán vortex street (Kármán, 1954), occurs over a range of Reynolds numbers (100 < Re < 150,000) wherein inertial forces are strong enough to drive the creation of

vortices, but viscous forces maintain coherence in the wake. The frequency and spacing of vortices shed by a cylinder may be controlled for experimentation by altering the flow velocity and cylinder diameter. The relationship between these parameters is articulated by the Strouhal number (St):

$$St = \frac{fd}{u}. \qquad (9)$$

where f is the expected vortex shedding frequency and d is the cylinder diameter. A rigid geometry in flow is characterized by a fixed Strouhal number for flows in the inertial regime. For instance, measurements of the shedding frequency at a controlled flow speed have St $\approx$ 0.2 (Schewe, 1983; Blevins, 1990). It follows that an increase in cylinder diameter or a decrease in speed creates a proportionate decrease in shedding frequency. Once shed, a vortex is carried downstream by the prevailing current. Studies that manipulate the Kármán street behind a bluff body have been used to investigate the effect of turbulence on flow sensing in swimming fish (see Section 4.5).

3 Stimulus Detection by Neuromasts

It is necessary to define what neuromasts are capable of sensing to differentiate the flow stimuli that matter to a fish. This is a subject that is explored extensively in subsequent chapters (van Netten & McHenry; Chagnaud & Coombs) and is therefore only summarized for the purposes of the present discussion. The superficial and canal neuromasts of the fish lateral line system operate in a similar manner (Fig. 6). For both, water motion generates drag on a microscopic gelatinous structure, called a cupula, that extends from the skin of a fish into the water. Embedded within the extracellular matrix of the cupula are the hair bundles, each of which originates from a single hair cell and includes microvilli (commonly called stereocilia) and a nonmotile kinocilium (see chapter by Webb). The hair bundles contain the molecular machinery for mechanotransduction (Hudspeth, 1982). Therefore, a change in the membrane potential of the hair cells is generated as the hair bundles bend in response to fluid forces on the cupula (Fig. 7). Depolarization in the membrane results in the release of neurotransmitter glutamate to increase the firing rate of action potentials in the afferent neurons that innervate the hair cells (Flock, 1965; Liao, 2010).

The cupula of a superficial neuromast projects from the surface of the body, where it is directly exposed to flow (Figs. 6b and 7). With rare exceptions (e.g., *Astyanax fasciatus*, Teyke, 1990), the cupula of a superficial neuromast is around 50 μm tall (Münz, 1989; Van Trump & McHenry, 2008), which generally resides within the boundary layer. For example, the boundary layer is 94 μm thick for a 36-Hz stimulus (Eq. 8), which is a frequency of maximal sensitivity in some species (Kroese & Schellart, 1992). This thickness increases to 1.4 mm at a position of 1 cm along the surface of the body (Eq. 5) for a gliding fish (see Section 2.2). This indicates that the boundary layer reduces the speed of flow that excites a superficial neuromast.
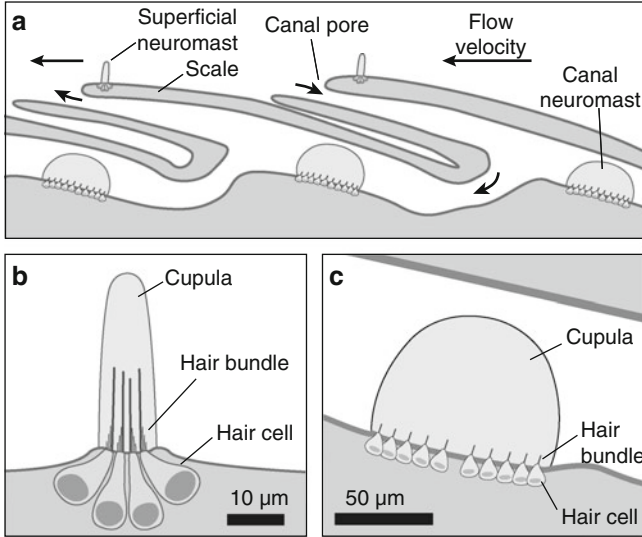
Fig. 6 The superficial and canal neuromasts of the lateral line system of fish. Schematic illustrations show (**a**) the relative position and major anatomical features of (**b**) superficial and (**c**) canal neuromasts. (**a**) The superficial neuromasts extend into the water surrounding the body, where they are directly exposed to water flow. Canal neuromasts are recessed in a channel beneath the scales, where they encounter flow when a pressure difference exists between the pores that open the channel to the surface (Weber & Schiewe, 1976; Kroese & Schellart, 1992). (**b**, **c**) Neuromasts consist of mechanosensory hair cells, a gelatinous cupula, and support cells (not shown). The hair bundle of each hair cell extends into the cupula and thereby detects deflections of the cupula created by fluid forces

The stimuli to which superficial neuromasts are sensitive may be considered in a variety of ways. Neurophysiological recordings of these receptors generally favor the notion that they are velocity sensitive (e.g., Görner, 1963), at least for frequencies below 50 Hz (Kroese & Schellart, 1992). As detailed in the chapter by van Netten and McHenry, this conclusion is consistent with our understanding for the biophysics of these receptors for frequencies above a few Hertz (see also Section 2.2). Viscous drag deflects the elastic hair cells within the cupula to generate its velocity sensitivity (McHenry et al., 2008). However, given the spatial variation in velocity that is created by the boundary layer and ambient flow conditions, it is not always apparent which velocity to consider as the stimulus for a superficial neuromast. For this reason, the shear stress at the surface (Eq. 3) can offer a more direct indication of the stimulus for these receptors (Rapo et al., 2009; Windsor & McHenry, 2009). The shear stress is proportional to viscosity and explicitly considers the velocity gradient (Eq. 3).

The position of a canal neuromast beneath the scales (Fig. 6c) enables these receptors to detect stimuli differently from superficial neuromasts. Although the cupula of a canal neuromast should also deflect in proportion to velocity due to viscous drag (Fig. 6a), this flow may be generated only when there is a pressure
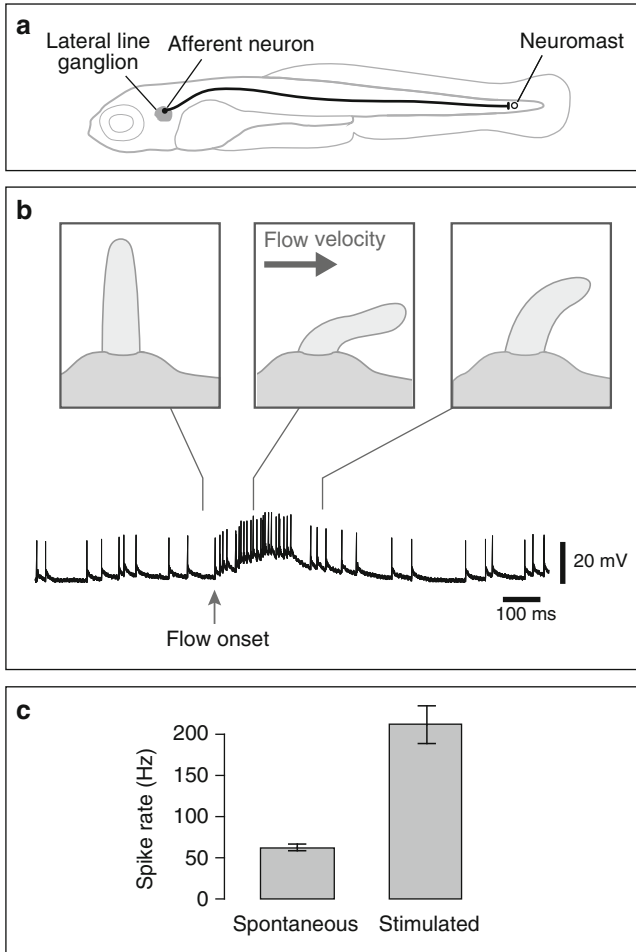
Fig. 7 Flow stimulus encoding by a lateral line afferent neuron (Liao, 2010). (**a**) Schematic illustration of the body of a 5-day old post-fertilization zebrafish larva with the location of an individual superficial neuromast and its innervation from a single afferent neuron highlighted. The cell body to this neuron resides within the lateral line ganglion. (**b**) A whole-cell patch recording from this cell body demonstrates the changes in the frequency of action potentials (i.e., spike rate) that are elicited by a microjet flow stimulus directed toward the P6 neuromast. Schematic drawings of the deflections of the cupula were traced from video-recordings of this experiment. (**c**) The mean values ($\pm$ 1 SE) of spike rate demonstrate a more than threefold increase above the spontaneous rate that was generated by the stimulus

difference at the pores that open the canal to the surface (Denton & Gray, 1989). In accordance with Euler's equation (Eq. 2), a pressure difference in a flow field may be generated by the acceleration of flow over the surface of the body. It is for this reason that a number of neurophysiological measurements have concluded that canal neuromasts function as acceleration detectors (Coombs & Montgomery, 1992;

Kroese & Schellart, 1992). However, pressure differences along the body may also be generated by spatial differences in velocity. This effect is apparent in the following expanded form of the Euler equation, which allows for spatial variation in velocity (Batchelor, 1967):

$$\frac{dp}{dx} = -\rho\left(\frac{du}{dt} + u\frac{du}{dx}\right). \tag{10}$$

This relationship demonstrates how the pressure gradient may vary with either flow acceleration (du/dt) or a spatial gradient in velocity ($u\,du/dx$). Therefore, it is more precise to define the stimulus for a canal neuromast as the pressure gradient over the body's surface or the pressure difference at the canal pores (Denton & Gray, 1988, 1989).

4 Case Studies

A deep understanding for flow sensing requires an explicit consideration of the stimuli to which the lateral line system is exposed. This notion is perhaps best illustrated by the prey localization behavior of predators. Investigators of this system have been able to interpret behavior in terms of the nervous stimuli generated by canal neuromasts, which may be predicted from a consideration of inviscid hydrodynamics. In contrast, obstacle detection by blind cavefish requires a consideration of viscous forces. The viscous boundary layer is also an essential component of flow sensing by larval prey fish when detecting a predator's strike. Despite these advances, it remains unresolved how flow stimuli are used by a fish to modulate swimming in still water and the Kármán gaiting adopted by fish in a turbulent flow field.

4.1 Prey Localization

Research on prey localization in fish offers the most comprehensive understanding of flow sensing in any animal. The mottled sculpin (*Cottus bairdi*) is a nocturnal predator that preys on swimming *Daphnia* in complete darkness. This is achieved by directing its approach toward the prey in the dark (Hoekstra & Janssen, 1985) and then capturing it with a suction feeding strike (Hoekstra & Janssen, 1986). Prey localization and capture require a functioning lateral line system (Hoekstra & Janssen, 1985), and this behavior can be elicited by a vibrating sphere stimulus in place of the prey (Coombs & Conley, 1997b). Therefore, the lateral line is both a necessary and sufficient sensory system for nocturnal predation in the mottled sculpin.
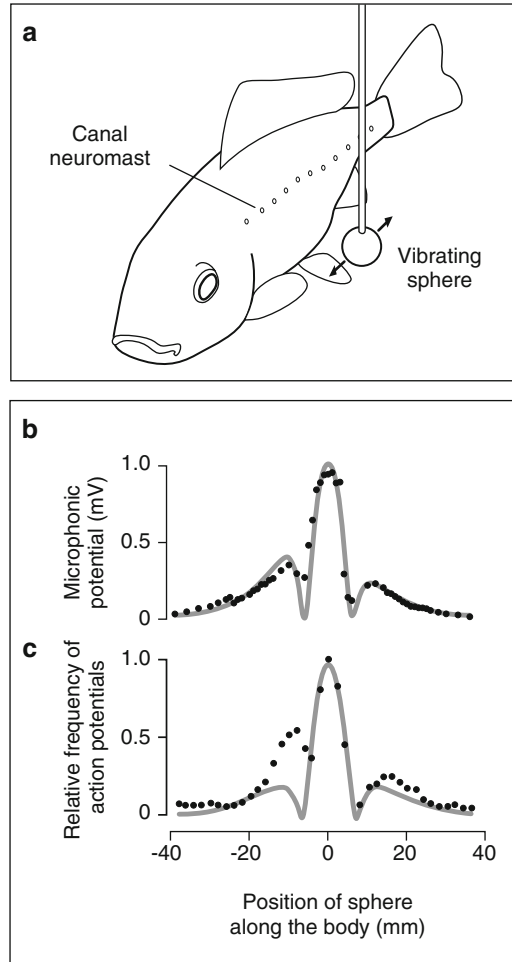
Fig. 8 Neurophysiology of prey localization. Recordings of the responses of neuromasts and lateral line afferent nerves to a vibrating sphere show a "Mexican hat" spatial pattern that may be predicted from hydrodynamic models. (**a**) These recordings were performed on anesthetized fish that were exposed to a vibrating sphere at a precisely controlled position with respect to the body. Plots show the amplitude of (**b**) microphonic potentials for individual neuromasts and (**c**) extracellular recordings of afferent fibers, which were recorded (circles) as a function of the position of the sphere along the length of the body. These patterns were predicted by the pressure gradient (gray line) generated by a dipole sphere. (**b**) The microphonic recordings were reported by Ćurčić-Blake and van Netten (2006) for a sphere positioned 1 cm away from the body of ruffe (body length: 10–13 cm). (**c**) Under similar experimental conditions, the relative afferent stimulus (which varies with the frequency of action potentials) was recorded in the goldfish (*Carassius auratus,* 9–12 cm) by Coombs et al. (1996)

The ability to stimulate the unconditioned predation behavior from a vibrating sphere has provided experimentalists with a critical tool for investigating the role of the lateral line system (Fig. 8a). The sphere offers a stimulus that is well controlled,

which has allowed for repeatable behavioral experiments and a neurophysiological preparation. These approaches have led to the finding that the variation in behavioral sensitivity with stimulus frequency follows the same trend as measured in the acceleration-sensitive fibers, but not velocity-sensitive fibers, in mottled sculpin (Coombs & Janssen, 1990). This suggests a dominant role for the canal neuromasts in mediating prey localization.

The stimuli detected by the canal neuromasts offer insight into an interesting feature of the prey localization behavior. Mottled sculpin exhibit the lowest accuracy at striking a vibrating sphere in the dark when they approach their target head-on. Strikes are significantly more accurate when approaching with an oblique body orientation that exposes the trunk lateral line to the source (Coombs & Conley, 1997b). This suggests that the trunk canal neuromasts offer enhanced spatial cues for localizing prey.

Major insight into these cues has emerged from mathematical models of the flow stimulus. The dipole pressure field generated by a vibrating sphere can be predicted from classic fluid dynamic theory that neglects the viscosity of the fluid (Kalmijn, 1988; Kalmijn 1989). Because of this inviscid assumption, the dipole model cannot predict boundary layer flows and hence the shear stress that stimulates the superficial neuromasts. However, this limitation does not matter to a consideration of the pressure gradients created by a vibrating sphere that stimulate the canal neuromasts (Fig. 8b, c). The extracellular potentials created by lateral line afferent neurons were recorded in the mottled sculpin for a range of positions of a vibrating sphere with respect to the body of an anesthetized fish. The frequency of action potentials that encode the intensity of flow was found to vary with a "Mexican hat" pattern as a function of the position of the sphere (Fig. 8c). A very similar spatial distribution is predicted for the amplitude of the pressure gradient in the mottled scuplin (Coombs & Conley, 1997a). This match between the flow model and neural response has been replicated in goldfish (*Carassius auratus*) (Coombs, 1994; Coombs et al., 1996; Goulet et al., 2008) and therefore appears in more than just nocturnal species. When this experiment was conducted in the ruffe (*Gymnocephalus cernuus* L.), the potentials generated by the hair cells of individual canal neuromasts were found to reflect closely the "Mexican hat" pattern (Fig. 8b, Ćurčić-Blake & van Netten, 2006). Further, computational fluid dynamics modeling (CFD) supported the assumption that viscosity may be neglected in models of dipole detection by the canal neuromasts (Rapo et al., 2009).

It remains unclear what cues are extracted from the array of neuromasts that determine the distance and orientation of a prey from a dipole field. The position of a vibrating sphere theoretically may be resolved through the use of a wavelet transformation (Ćurčić-Blake & van Netten, 2006) or from the zero-crossings and peaks in values of pressure gradient (Goulet et al., 2008) detected by the superficial neuromast stimuli. However, the spatial activation pattern varies in a complex way—not only with source position, but also source distance and orientation. Behavioral experiments to manipulate these factors revealed that the ability of mottled sculpin to determine source position is not guided by amplitude peaks (Coombs and Patton, 2009). Moreover, investigations into the central processing of

the lateral line system have yet to distinguish what cues are derived from this spatial pattern of stimuli (Bleckmann, 2008; see also the chapter by Bleckmann & Mogdans).

4.2 Obstacle Detection

The success of inviscid flow theory in modeling prey localization (Fig. 8b, c) appears to suggest that canal neuromasts are uninfluenced by the viscosity of water. This idea was put to the test with mathematical models of obstacle detection in the Mexican blind cavefish (*Astyanax mexicanus*). These animals use their lateral line system to sense changes in self-generated flow to avoid colliding with obstacles (Windsor et al., 2008). The hydrodynamic disturbances generated by these obstacles have been modeled with both an inviscid potential flow model (Hassan, 1985; 1992a,b) and a CFD model that included viscosity (Windsor et al., 2010a,b) (Fig. 9).

Both models considered the flow generated on the surface of the body as it glides toward and along a flat wall. A comparison of their results shows that the magnitude and pattern of the predicted pressure gradient differ substantially when viscosity is included. For example, when gliding along a wall, the CFD model predicts a change in pressure on the surface of the body that is more than 50 times greater than what is predicted by the potential flow model (Windsor et al., 2010a). Furthermore, the CFD model exhibits a substantially greater elevation in the pressure gradient as the distance decreases between the fish and the wall. Unlike the potential flow model, the CFD model can predict how the boundary layer around the body of a gliding fish is altered by its interaction with the wall. This demonstrates that the viscous interaction between the wall and the fish can substantially affect the pressure gradient on the surface of the fish's body. This finding holds even at high Reynolds numbers (Re = 6000), where one might predict a negligible contribution from viscosity. Therefore, the viscosity of water can influence flow sensing, even in flow that is governed largely by inertial hydrodynamics.

4.3 Predator Evasion

Although viscosity may be entirely neglected (e.g., prey localization) or have an indirect effect (e.g., obstacle detection) on the stimuli detected by canal neuromasts, viscous fluid dynamics are fundamental to sensing by superficial neuromasts. Creating a stimulus that may be detected by these receptors requires water motion relative to the body of a fish. Relative flow velocity is created in larval fish when attacked by a suction-feeding predator, which triggers a fast-start escape response in the larva to evade capture (McHenry et al., 2009).
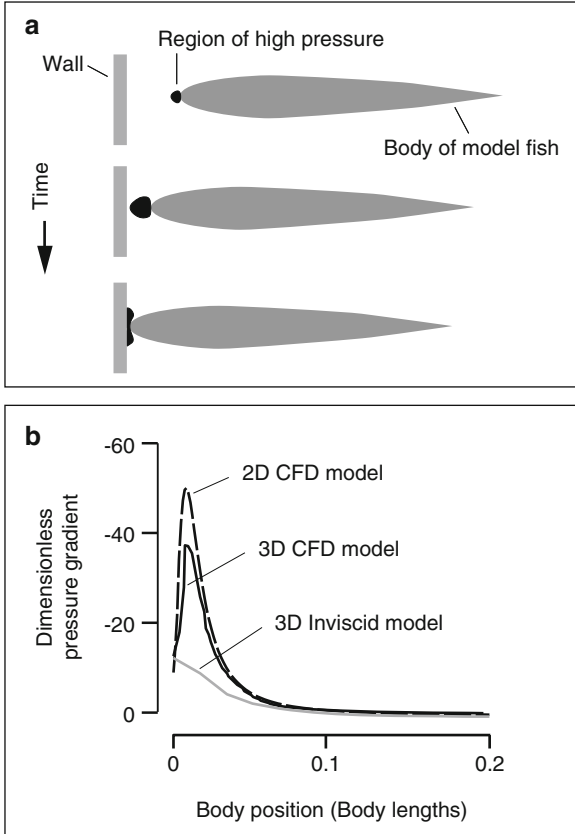
Fig. 9 Mathematical models of the flow around a Mexican blind cavefish as it glides toward a wall. This event has been modeled with potential flow theory (3D Inviscid model: Hassan, 1992) that neglects viscosity and computational fluid dynamics (CFD) models in 2D and 3D that include viscosity (Windsor et al., 2010). (**a**) Simulations of the approach (Re = 6000) reveal a region of high pressure (black shape) at the anterior-most point on the body that spreads laterally as the body approaches the wall. (**b**) The pressure gradient, the stimulus detected by canal neuromasts, predicted by this event differs between mathematical models. The 3D CFD model (black line) predicts a smaller maximum value than the 2D CFD model (dashed line), but a much greater value than the inviscid model (gray line). This demonstrates a case in which viscosity influences the flow stimulus for the canal neuromasts

Suction feeding is achieved by the rapid expansion of a predator's buccal cavity. This motion creates low pressure that accelerates water into the mouth with the funnel-shaped streamlines (Fig. 10a). Despite this complexity to the flow field, velocities directly in front of the mouth are nearly laminar and therefore relatively simple (Ferry-Graham et al., 2003; Higham et al., 2005). Because prey are generally targeted at this location, it is appropriate to apply the Euler equation (Eq. 10) to calculate changes in flow for a prey (Wainwright & Day, 2007). This flow may
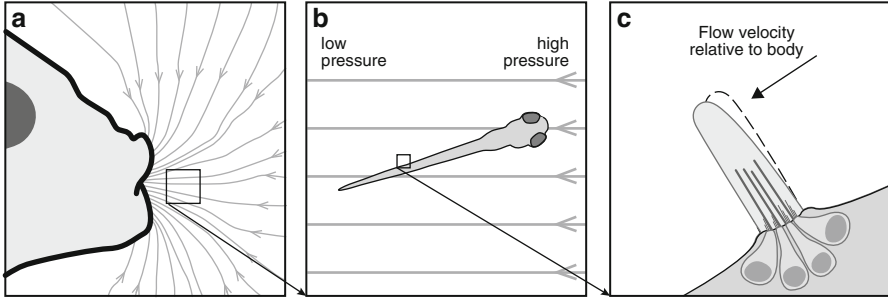
Fig. 10 Predator detection by a prey fish. (**a**) The flow field generated by a suction feeding sunfish (*Lepomis macrochirus,* shown from a lateral view) is illustrated with streamlines measured with particle tracking velocimetry (Higham et al., 2005). (**b**) Like the surrounding water, a fish prey (drawn as a larva from a dorsal view) is drawn toward the predator due to the low pressure generated by suction. (**c**) The flow velocity relative to the body is sensed by the deflection of the superficial neuromasts (Stewart & McHenry, 2010)

be approximated under experimental conditions that expose larval prey to a pressure gradient at a controlled rate to stimulate the escape response (McHenry et al., 2009).

For a larval fish exposed to this stimulus, flow acceleration is inversely proportional to density for both the body of a prey fish and the water. Therefore, the flow velocity relative to the prey depends on the density of the prey (ρ_{body}) relative to the water (ρ_{water}), as indicated by the specific gravity (SG $= \rho_{body}/\rho_{water}$). By modeling the relative flow predicted from measurements of specific gravity, the flow velocity of a predator's strike is substantially attenuated by the larva's body being carried along with the water. This is indicated by the maximum flow velocity from the larva's frame of reference during a strike, which is a small fraction ($<6\%$) of the value from the earth-bound frame of reference. Further, subtle variation in the specific gravity can have a large influence on relative flow. For example, the specific gravity decreases by about 5% when the gas bladder inflates in zebrafish larvae (*Danio rerio*), at 4–5 days after fertilization, which causes the maximum relative velocity to decrease by 80% (Stewart & McHenry, 2010). Therefore, the ability of a larval fish to sense a predator is governed by a fluid–structure interaction between the body and flow field.

4.4 Propulsion

It is an old speculation that the lateral line system influences how a fish coordinates the kinematics of freestream swimming (Schulze, 1870). If such a mechanism exists, then it is not qualitatively apparent from watching the swimming of a fish that has had its lateral line system ablated (Dijkgraaf, 1963). Instead, the lateral line could provide stimuli that allow a fish to subtly tune its swimming to reduce the drag on the body. One version of this idea was formulated as the active drag reduction hypothesis (Lighthill, 1995).

The active drag reduction hypothesis is supported by research on clupeoid fishes. These animals possess a modified canal system that is considered to be highly sensitive to differences in pressure across the cranium (Denton & Gray, 1983, 1993). For this reason, a potential flow model of these pressure differences was devised to determine how this stimulus could influence swimming kinematics to minimize drag (Lighthill, 1993). This model predicts that drag should be minimized when the yaw angle of the head oscillates in phase with its lateral velocity. In addition, the optimal amplitude of changes in yaw and lateral velocity may be predicted from the shape of the fish's head. Measurements of the kinematics of swimming in Atlantic herring, a clupeoid species (*Clupea harengus* L.), supported these predictions (Rowe et al., 1993). However, these predictions were not supported by the kinematics of the golden shiner (*Notemigonus crysoleucas*), which does not school as strongly as clupeoid species. The golden shiner swims with head kinematics that do not minimize drag, and ablating the lateral line system does not elevate drag (McHenry et al., 2010). Although these results suggest that fish do not generally use the lateral line system to minimize pressure differences on the head, it remains possible that flow stimuli can be used to tune swimming kinematics in other ways. For example, lateral line inputs may assist in stabilizing swimming under turbulent conditions (Liao, 2006), or separation in the boundary layer may be avoided by sensory feedback (Anderson et al., 2001).

One of the challenges to understanding the role of the lateral line system in swimming is determining the stimuli detected by the neuromasts during locomotion. Measurements of the boundary layer over the surface of a swimming fish (Fig. 11) offer a glimpse into the stimuli detected by the superficial neuromasts (Fig. 3) (Anderson et al., 2001). Like the flow over a plate (Fig. 3d), the shear stress over the body is greatest near its leading edge, followed by a monotonic decline. This indicates that viscous drag and the stimulus detected by the superficial neuromasts is greatest in the anterior region of the body. However, the thickness of a fish's body and the flow created for propulsion influence the boundary layer, such that it deviates from flow over a plate. For example, skin friction remains elevated in the cranial region, anterior to the widest region of the body (Fig. 10b), rather than the precipitous drop-off seen in a flat plate (Fig. 3c). Therefore, an examination of the flow stimuli during locomotion requires experimental or theoretical approaches that extend beyond the simple cases considered by classical theory.

4.5 Kármán Gaiting

A broad diversity of fishes inhabit turbulent environments, and this variation in flow can have a strong influence on swimming behavior (Webb, 1998). Perhaps the most dramatic example is offered by the Kármán gait (Liao et al., 2003a), which is the synchronization of swimming kinematics to vortices in a Kármán vortex street (Fig. 12a).
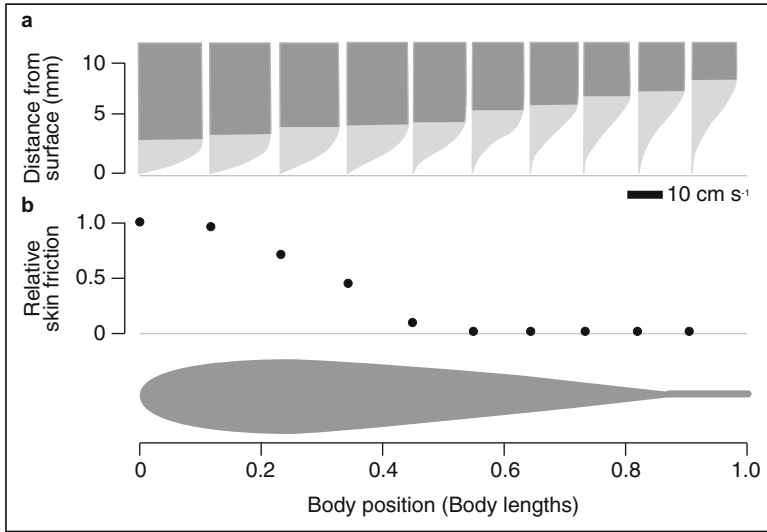
Fig. 11 Boundary layers over the surface of the body (length = 9 cm) of a swimming scup, *Stenotomus chrysops* (Anderson et al., 2001). (**a**) Flow velocities were measured by particle tracking velocimetry from a series of recordings. These profiles allow for the calculation of (**b**) skin friction (Eq. 3) on the surface of the body, which is normalized by the maximum value. These measurements demonstrate how the anterior half of the body is the major site of viscous drag production and offers a substantially stronger stimulus for the superficial neuromasts. The silhouette of the body of the fish from a dorsal view (in gray) illustrates the approximate shape of the body

When Kármán gaiting behind a cylinder, rainbow trout (*Oncorhynchus mykiss*) exhibit a lower tailbeat frequency and larger lateral body amplitude and curvature than seen during swimming in uniform flow of comparable velocity (Liao et al., 2003b). Simultaneous visualization of the flow and fish motions show that the body slaloms between oncoming vortices, moving with the lateral component of the sinusoidal flow rather than actively swimming through each vortex center (Fig. 12a). This motion is the result of a shift in the timing of lateral body motion relative to the vortices that pass along the body. For example, the center of mass oscillates antiphase (i.e., 180° phase shift) to move to its farthest lateral distance from a vortex core as it passes that body position (Fig. 12b). This slaloming is further facilitated by the head's motion away from a vortex (100° phase shift) and the tail moving toward the vortex as it approaches (230° phase shift).

Kármán gaiting emerges from a fluid–structure interaction between the body of the fish and the forces generated by the wake. Muscle recordings in trout revealed that only the anterior red muscles in the trunk are reliably activated during this behavior. This low level of muscle activity suggests that muscles primarily play a role in controlling body posture and stiffness (Liao, 2004). In contrast, trout swimming in freestream flow exhibit propagating waves of muscle activity along the whole body that serve to power body undulation. In addition, trout in a Kármán
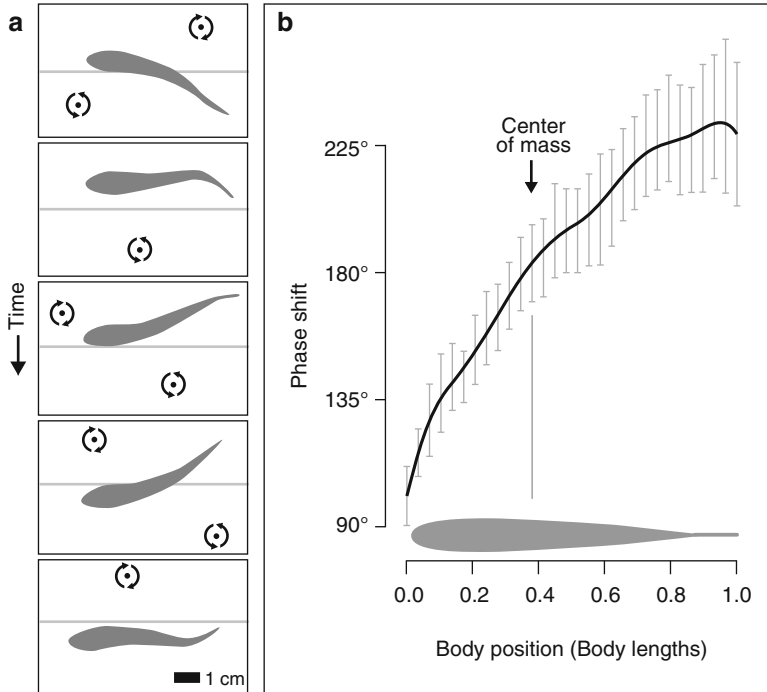
Fig. 12 Trout (*Oncorhynchus mykiss*) adopt a Kármán gait when holding station in a vortex street in the wake of an obstacle in flow. (**a**) A dorsal view of the body of the trout (in gray) illustrates the slaloming around vortices (centered at the rotating arrows) that is characteristic of this gait, measured in the wake of a semicylinder (Liao et al., 2003b). The centers of vortices (see Fig. 5) were measured with particle tracking velocimetry and the kinematics of swimming were recorded simultaneously. (**b**) These measurements revealed that the phase shift of lateral undulations is coordinated with respect to vortex shedding. Mean values (± 1 SE) for the phase shift demonstrate that the center of mass oscillates in antiphase (i.e., 180°) with the vortices and that the anterior and posterior regions are respectively directed away and toward the passing vortex

street at times actively move their pectoral fins to enable them to hold station without any muscle activity in the trunk. This demonstrates that Kármán gaiting can balance thrust and drag solely through fin action and the intrinsic compliance of the musculoskeletal system (Liao et al., 2003a,b).

Respirometry measurements demonstrated that Kármán gaiting allows a fish to use less oxygen when swimming. This indicates that fish can use some of the energy of environmental vortices to passively generate thrust (Taguchi & Liao, 2011). It has been proposed that the lateral translation of the body and its angular changes due to the vortex street may allow the body to act as a sail and thereby tack upstream passively (Liao et al., 2003a). This idea is supported by experimental and theoretical research on the hydrodynamics of fish-like foils, which can generate thrust when placed in oscillating flow (Wu & Chwang, 1975; Beal, 2003). Consequently, a dead trout towed behind a cylinder can passively generate thrust and move upstream on a slack line when they happen to synchronize with vortices

(Liao, 2004; Beal et al., 2006). Therefore, no muscle activity is required to maintain station, or even move upstream, in a vortex street if a body has the appropriate compliance.

The lateral line system plays a role in coordinating the Kármán gait. This was indicated by experiments that blocked the lateral line system by treating trout with a solution of cobalt chloride (Karlsen & Sand, 1987). This treatment altered the kinematics of Kármán gaiting (Liao, 2006), relative to control animals. Trout with a blocked lateral line exhibited faster body wave speed, lower maximum body curvature, lower tail-beat amplitude, and a longer and more variable body wavelength. It is unclear whether this effect may be attributed to stimuli detected by canal or superficial neuromasts. Similar experiments demonstrated that the lateral line is necessary to entrain in the relatively stable, low-pressure suction region directly behind a cylinder (Sutterlin & Waddy, 1975; Montgomery et al., 2003). Trout swimming under illuminated conditions choose to spend most of their time swimming in a turbulent vortex street, even with a blocked lateral line. In contrast, this behavior is rarely exhibited in the same species when swimming in the dark (Liao, 2006). Therefore, the lateral line system plays a role in the *ability* to Kármán gait and the visual system appears to be important in the *preference* of fish to exhibit this behavior.

5 Summary

Hydrodynamics provides a basis for understanding the stimuli detected by the lateral line system. Models of these stimuli have employed inviscid hydrodynamic theory (Kalmijn, 1988), which can accurately predict some stimuli detected by canal neuromasts (e.g., Coombs et al., 1996). However, there are circumstances where viscosity influences the flow detected by canal neuromasts (e.g., Fig. 11b) and viscous boundary layers are essential to the functioning of superficial neuromasts (McHenry et al., 2008). It is therefore fortuitous that computational modeling (e.g., Rapo et al., 2009) and flow visualization techniques (e.g., Anderson et al., 2001) are increasingly practical approaches for biological investigation. Studies adopting these techniques would do well to involve more natural levels of noise and turbulence in the environment. The integration of biomechanics with neurophysiological and behavioral approaches offers great promise for a deeper understanding of the lateral line system.

References

Anderson, E. J., McGillis, W. R., & Grosenbaugh, M. A. (2001). The boundary layer of swimming fish. *Journal of Experimental Biology*, 204, 81–102.
Anderson, J. M. (1996). Vorticity control for efficient propulsion. In *Applied ocean science engineering, MIT* (pp. 1–193). Cambridge: MIT/Woods Hole Oceanographic Institution.

Batchelor, G. (1967). *An introduction to fluid dynamics*. New York: Cambridge University Press.

Beal, D. N. (2003). *Propulsion through wake synchronization using a flapping foil.* Doctoral Dissertation, Massachusetts Institute of Technology.

Beal, D. N., Hover, F. S., Triantafyllou, M. S., Liao, J. C., & Lauder, G. V. (2006). Passive propulsion in vortex wakes. *Journal of Fluid Mechanics, 549,* 385–402.

Bleckmann, H. (2008). Peripheral and central processing of lateral line information. *Journal of Comparative Physiology A*, 194, 145–158.

Blevins, R. D. (1990). *Flow induced vibration,* 2nd ed. Malabar, FL: Krieger..

Coombs, S. (1994). Nearfield detection of dipole sources by the goldfish (*Carassius auratus*) and the mottled sculpin (*Cottus bairdi*). *Journal of Experimental Biology*, 190, 109–129.

Coombs, S., & Janssen, J. (1990). Behavioral and neurophysiological assessment of lateral line sensitivity in the mottled sculpin, *Cottus-bairdi*. *Journal of Comparative Physiology A*, 167, 557–567.

Coombs, S., & Montgomery, J. C. (1992). Fibers innervating different parts of the lateral line system of an antarctic notothenioid, *Trematomus-Bernacchii*, have similar frequency responses, despite large variation in the peripheral morphology. *Brain Behavior and Evolution*, 40, 217–233.

Coombs, S., & Conley, R. A. (1997a). Dipole source localization by the mottled sculpin. 2. The role of lateral line excitation patterns. *Journal of Comparative Physiology A*, 180, 401–415.

Coombs, S., & Conley, R. A. (1997b). Dipole source localization by mottled sculpin. 1. Approach strategies. *Journal of Comparative Physiology A, 180,* 387–399

Coombs, S., & Patton, P. (2009). Lateral line stimulation patterns and prey orienting behavior in the Lake Michigan mottled sculpin (*Cottus bairdi*). *Journal of Comparative Physiology A*, 195, 279–297.

Coombs, S., Hasting, M., & Finneran, J. (1996). Modeling and measuring lateral line excitation patterns to changing dipole source locations. *Journal of Comparative Physiology A*, 178, 359–371.

Ćurčić-Blake, B., & van Netten, S. M. (2006). Source location encoding in the fish lateral line canal. *Journal of Experimental Biology*, 209, 1548–1559.

Daniel, T. (1981). Fish mucus: *In situ* measurements of polymer drag reduction. *Biological Bulletin,* 160, 376–382.

Denton, E. J., & Gray, J. A. B. (1983). Mechanical factors in the excitation of clupeid lateral lines. *Proceedings of the Royal Society B: Biological Sciences,* 218, 1–26.

Denton, E. J., & Gray, J. A. B. (1988). Mechanical factors in the excitation of the lateral lines of fishes. In J. Atema, R. R. Fay, A. N. Popper, & W. N. Tavolga (Eds.), *Sensory biology of aquatic animals*(pp. 595–618). New York: Springer.

Denton, E. J., & Gray, J. A. B. (1989). Some observations on the forces acting on neuromasts in fish lateral line canals. In S. Coombs, P. Görner, & H. Münz (Eds.), *The mechanosensory lateral line: Neurobiology and evolution* (pp. 79–97). New York: Springer-Verlag.

Denton, E. J., & Gray, J. A. B. (1993). Stimulation of the acoustico-lateralis system of clupeid fish by external sources and their own movements. *Philosophical Transactions: Biological Sciences,* 341, 113–127.

Dijkgraaf, S. (1963). The functioning and significance of lateral-line organs. *Biological Reviews of the Cambridge Philosophical Society*, 38, 51–105.

Dinklo, T. (2005). *Mechano- and electrophysiological studies on cochlear hair cells and superficial lateral line cupulae*. Doctoral dissertation, University of Groningen.

Ferry-Graham, L. A., Wainwright, P. C., & Lauder, G. V. (2003). Quantification of flow during suction feeding in bluegill sunfish. *Zoology*, 106, 159–168.

Flock, Å. (1965). Transducing mechanisms in lateral line canal organ receptors. *Cold Spring Harbor Symposia on Quantitative Biology*, 30, 133–145.

Görner, P. (1963). Untersuchungen zur Morphologie und Elektrophysiologie des Seitenlinienorgans vom Krallenfrosch (*Xenopus laevis* Daudin). *Journal of Comparative Physiology A*, 47, 316–338.

Goulet, J., Engelmann, J., Chagnaud, B. P., Franosch, J.-M. P., Suttner, M. D., & Hemmen, J. L. (2008). Object localization through the lateral line system of fish: Theory and experiment. *Journal of Comparative Physiology A*, 194, 1–17.

Hassan, E. S. (1985). Mathematical analysis of the stimulus of the lateral line organ. *Biological Cybernetics*, 52, 23–36.

Hassan, E. S. (1992a). Mathematical description of the stimuli to the lateral line system of fish derived from a three-dimensional flow field analysis. II. The case of gliding alongside or above a plane surface. *Biological Cybernetics*, 66, 453–461.

Hassan, E. S. (1992b). Mathematical description of the stimuli to the lateral line system of fish derived from a three-dimensional flow field analysis. I. The cases of moving in open water and of gliding towards a plane surface, *Biological Cybernetics,* 66, 443–452.

Higham, T. E., Day, S. W., & Wainwright, P. C. (2005). Sucking while swimming: Evaluating the effects of ram speed on suction generation in bluegill sunfish *Lepomis macrochirus* using digital particle image velocimetry. *Journal of Experimental Biology,* 208, 2653–2660.

Hoekstra, D., & Janssen, J. (1985). Non-visual feeding behavior of the mottled sculpin, *Cottus bairdi*, in Lake Michigan. *Environmental Biology of Fishes,* 12, 111–117.

Hoekstra, D., & Janssen, J. (1986). Lateral line receptivity in the mottled sculpin. *Copeia*, 1986, 91–96.

Hudspeth, A. J. (1982). Extracellular current flow and the site of transduction by vertebrate hair cells. *Journal of Neuroscience*, 2, 1–10.

Kalmijn, A. J. (1988). Hydrodynamic and acoustic field detection. In J. Atema, R. R. Fay, A. N. Popper, & W. N. Tavolga (Eds.), *Sensory biology of aquatic animals*. (pp. 83–130). New York: Springer-Verlag.

Kalmijn, A. J. (1989). Functional evolution of lateral line and inner ear sensory systems. In S. Coombs, P. Görner, & H. Münz (Eds.), *The mechanosensory lateral line: Neurobiology and evolution* (pp. 187–215). New York: Springer-Verlag.

Karlsen, H. E., & Sand, O. (1987). Selective and reversible blocking of the lateral line in freshwater fish. *Journal of Experimental Biology*, 133, 249–262.

Kármán, von, T. (1954). *Aerodynamics: Selected topics in the light of their historical development*. Ithaca, NY: Cornell University Press.

Kroese, A. B. A., & Schellart, N. A. M. (1992). Velocity-sensitive and acceleration-sensitive units in the trunk lateral line of the trout. *Journal of Neurophysiology*, 68, 2212–2221.

Liao, J. C. (2004). Neuromuscular control of trout swimming in a vortex street: Implications for energy economy during the Kármán gait. *Journal of Experimental Biology*, 207, 3495–3506.

Liao, J. C. (2006). The role of the lateral line and vision on body kinematics and hydrodynamic preference of rainbow trout in turbulent flow. *Journal of Experimental Biology,* 209, 4077–4090.

Liao, J. C. (2010). Organization and physiology of posterior lateral line afferent neurons in larval zebrafish. *Biology Letters, 6,* 402–405.

Liao, J. C., Beal, D. N., Lauder, G. V., & Triantafyllou, M. S. (2003a). The Kármán gait: Novel body kinematics of rainbow trout swimming in a vortex street. *Journal of Experimental Biology,* 206, 1059–1073.

Liao, J. C., Beal, D. N., Lauder, G. V., & Triantafyllou, M. S. (2003b). Fish exploiting vortices decrease muscle activity. *Science*, 302, 1566–1569.

Lighthill, J. (1993). Estimates of pressure differences across the head of a swimming clupeid fish. *Philosophical Transactions: Biological Sci*ences, 341, 129–140.

Lighthill, J. (1995). The role of the lateral line in active drag reduction by clupeoid fishes. *Animal Locomotion Symposium by the Society for Experimental Biology,* 49, 35–48.

McHenry, M. J., Strother, J. A., & van Netten, S. M. (2008). Mechanical filtering by the boundary layer and fluid-structure interaction in the superficial neuromast of the fish lateral line system. *Journal of Comparative Physiology A*, 194, 795–810.

McHenry, M. J., Feitl, K. E., Strother, J. S., & Van Trump, W. J. (2009). Larval zebrafish rapidly sense the water flow of a predator's strike. *Biology Letters,* 5, 477–497.

McHenry, M. J., Michel, K. B., & Stewart, W. J. (2010). Hydrodynamic sensing does not facilitate active drag reduction in the golden shiner (*Notemigonus crysoleucas*). *Journal of Experimental Biology,* 213, 1309–1319.

Montgomery, J. C., McDonald, F., Baker, C. F., Carton, A. G., & Ling, N. (2003). Sensory integration in the hydrodynamic world of rainbow trout. *Proceedings of the Royal Society B: Biological Sciences,* 270, S195–S197.

Muddada, S., & Patnaik, B. S. V. (2011). Understanding complex systems. In S. Banerjee, M. Mitra, & L. Rondoni (Eds.), *Understanding complex systems* (pp. 87–136). Berlin: Springer.

Mönz, H. (1989). Functional organization of the lateral line periphery. In S. Coombs, P. Görner, & H. Münz (Eds.). *The mechanosensory lateral line: Neurobiology and Evolution* (pp. 285–297). New York: Springer-Verlag.

Prandtl, L. (1904). Über Flüssigkeitsbewegung bei sehr kleiner Reibung. *Proceedings Third International Kongreß Heidelberg*, S, 484–491.

Rapo, M. A., Jiang, H., & Grosenbaugh, M. A. (2009). Using computational fluid dynamics to calculate the stimulus to the lateral line of a fish in still water. *Journal of Experimental Biology,* 212, 1494–1505.

Reynolds, O. (1883). An experimental investigation of the circumstances which determine whether the motion of water shall be direct or sinuous, and the law of resistance in parallel channels. *Philosophical Transactions of the Royal Society*, 174, 935–982.

Rowe, D. M., Denton, E. J., & Batty, R. S. (1993). Head turning in herring and some other fish. *Proceedings of the Royal Society B: Biological Sciences*, 341, 141–148.

Schewe, G. (1983). On the force fluctuations acting on a circular cylinder in crossflow from subcritical up to transcritical Reynolds numbers. *Journal of Fluid Mechanics,* 133, 265–285.

Schlichting, H. (1979). *Boundary-layer theory*. New York: Springer-Verlag.

Schulze, F. E. (1870). Über die Nervenendigung in den sogenannten Schleimkanälen der Fische und über entsprechende Organe der durch Kiemen athmenden Amphibien. *Archive für Anatomische Physiologie Leipzig*, 759–769.

Stewart, W. J., & McHenry, M. J. (2010). Sensing the strike of a predator fish depends on the specific gravity of a prey fish. *Journal of Experimental Biology*, 213, 3769–3777.

Sutterlin, A., & Waddy, S. (1975). Possible role of posterior lateral line in obstacle entrainment by brook trout (*Salvelinus-Fontinalis*). *Journal of Fisheries Research Board of Canada*, 32, 2441–2446.

Taguchi, M., & Liao, J. C. (2011). Rainbow trout consume less oxygen in turbulence: The energetics of swimming behaviors at different speeds. *Journal of Experimental Biology,* 214, 1428–1436.

Teyke, T. (1990).Morphological differences in neuromasts of the blind cave fish *Astyanax hubbsi* and the sighted river fish *Astyanax mexicanus*. *Brain Behavior and Evolution*, 35, 23–30.

Van Dyke, M. (1982). *An album of fluid motion*. Palo Alto, CA: Parabolic Press.

van Netten, S. M. (2006). Hydrodynamic detection by cupulae in a lateral line canal: Functional relations between physics and physiology. *Biological Cybernetics*, 94, 67–85.

Van Trump, W. J., & McHenry, M. J. (2008). The morphology and mechanical sensitivity of lateral line receptors in zebrafish larvae (*Danio rerio*). *Journal of Experimental Biology,* 211, 2105–2115.

Wainwright, P. C., & Day, S. W. (2007). The forces exerted by aquatic suction feeders on their prey. *Journal of the Royal Society Interface*, 4, 553–560.

Webb, P. W. (1998). Entrainment by river chub *Nocomis micropogon* and smallmouth bass *Micropterus dolomieu* on cylinders. *Journal of Experimental Biology*, 201, 2403–2412.

Weber, D. D., & Schiewe, M. H. (1976). Morphology and function of the lateral line of juvenile steelhead trout in relation to gas-bubble disease. *Journal of Fish Biology,* 9, 217–233.

Windsor, S. P., & McHenry, M. J. (2009). The influence of viscous hydrod3842ynamics on the fish lateral-line system. *Integrative and Comparative Biology*, 49, 691–701.

Windsor, S. P., Tan, D., & Montgomery, J. C. (2008). Swimming kinematics and hydrodynamic imaging in the blind Mexican cave fish (*Astyanax fasciatus*). *Journal of Experimental Biology,* 211, 2950–2959.

Windsor, S., Norris, S., & Cameron, S. (2010a). The flow fields involved in hydrodynamic imaging by blind Mexican cave fish (*Astyanax fasciatus*). Part I: Open water and heading towards a wall. *Journal of Experimental Biology,* 213, 3819–3831.

Windsor, S., Norris, S. E., Cameron, S. M., Mallinson, G. D., & Montgomery, J. C. (2010b). The flow fields involved in hydrodynamic imaging by blind Mexican cave fish (*Astyanax fasciatus*). Part II: Gliding parallel to a wall. *Journal of Experimental Biology,* 213, 3832–3842.

Wu, T. Y., & Chwang, A. T. (1975). *Extraction of flow energy by fish and birds in a wavy stream.* New York: Plenum Press.